Chin. Phys. Lett. **39**, 047401 (2022)

# A New Superconductor Parent Compound $NaMn_6Bi_5$ with Quasi-One-Dimensional Structure and Lower Antiferromagnetic-Like Transition Temperatures

Ying Zhou(周颖)[1,2†], Long Chen(陈龙)[1,2†], Gang Wang(王刚)[1,2,3*], Yu-Xin Wang(王郁欣)[1,2], Zhi-Chuan Wang(王志川)[1,2], Cong-Cong Chai(柴聪聪)[1,2], Zhong-Nan Guo(郭中楠)[4], Jiang-Ping Hu(胡江平)[1,2,3*], and Xiao-Long Chen(陈小龙)[1,2,3*]

[1]*Beijing National Laboratory for Condensed Matter Physics, Institute of Physics, Chinese Academy of Sciences, Beijing 100190, China*
[2]*University of Chinese Academy of Sciences, Beijing 100049, China*
[3]*Songshan Lake Materials Laboratory, Dongguan 523808, China*
[4]*Department of Chemistry, School of Chemistry and Biological Engineering, University of Science and Technology Beijing, Beijing 100083, China*

(Received 5 February 2022; accepted 24 February 2022; published online 9 March 2022)

Mn-based superconductors are very rare and their superconductivity has only been reported in three-dimensional MnP and quasi-one-dimensional $KMn_6Bi_5$ and $RbMn_6Bi_5$ with $[Mn_6Bi_5]^-$ columns under high pressures. Here we report the synthesis, magnetism, electrical resistivity, and specific heat capacity of the newly discovered quasi-one-dimensional $NaMn_6Bi_5$. Compared with other $AMn_6Bi_5$ ($A$ = K, Rb, and Cs), $NaMn_6Bi_5$ has abnormal Bi–Bi bond lengths and two antiferromagnetic-like transitions at 47.3 K and 51.8 K. Anisotropic resistivity and low-temperature non-Fermi liquid behavior are observed. Heat capacity measurement reveals that the Sommerfeld coefficient for $NaMn_6Bi_5$ is unusually large. Using first-principles calculations, an unusual enhancement of density of states near the Fermi level is demonstrated for $NaMn_6Bi_5$. The features make $NaMn_6Bi_5$ a more suitable platform to explore the interplay of magnetism and superconductivity.

DOI: 10.1088/0256-307X/39/4/047401

Cuprates,[1–4] iron pnictides,[5–7] and heavy-fermion superconductors[8,9] are unconventional superconductors violating the Bardeen–Cooper–Schrieffer (BCS) theory and provide ample opportunity to advance our understanding of physics of strong-correlated systems in the past decades. Apart from cuprates and iron pnictides, other 3*d* transition metal based compounds are also of great interest in exploring superconductors for varying crystal fields of 3*d* transition metal centered polyhedra[10,11] and unique magnetism.[12,13] By suppressing the magnetism of 3*d* transition metal based compounds, unconventional superconductivity is expected to emerge in the vicinity of antiferromagnetic (AFM) quantum critical point.[14] However, up to date, only a few other 3*d* transition metal based superconductors, such as Cr-based,[15–19] Mn-based[20,21] and Ni-based[22,23] superconductors, have been reported.

The first Mn-based superconductor was reported in three-dimensional MnP with its helical magnetic order suppressed under pressures,[20,21] which suggests that superconductivity emerges in Mn-based systems by suppressing the helical magnetic order. $KMn_6Bi_5$ is a quasi-one-dimensional ternary Mn-based compound with unique $[Mn_6Bi_5]^-$ columns[24] and an interesting helical magnetic order was predicted in its sister compound $RbMn_6Bi_5$ in our previous work.[25] Very recently, Cheng *et al.*[26,27] reported the pressure-induced superconductivity with transition temperature up to 9.3 K in $KMn_6Bi_5$ and 9.5 K in $RbMn_6Bi_5$ by suppressing the AFM order, which open a new avenue for finding more Mn-based superconductors.

Following $RbMn_6Bi_5$, we have substituted Rb by other alkali metals including Na and Cs and obtained $NaMn_6Bi_5$ having lower AFM-like transition temperatures. Here, the single crystal growth, magnetism, and transport properties of $NaMn_6Bi_5$ are reported. For the smaller Na, $NaMn_6Bi_5$ shares a similar quasi-one-dimensional structure motif $[Mn_6Bi_5]^-$ as those of $KMn_6Bi_5$ and $RbMn_6Bi_5$, but having some abnormal Bi–Bi bond lengths. The lowering AFM-like transition temperature is confirmed by magnetic susceptibility, resistivity, and specific heat capacity measurements. Meanwhile, anisotropic resistivity, non-Fermi liquid behavior, and largely enhanced Sommerfeld coefficient are observed. First-principles calculations re-

†These authors contributed equally to this work.
*Corresponding authors. Email: gangwang@iphy.ac.cn; jphu@iphy.ac.cn; xlchen@iphy.ac.cn
© 2022 Chinese Physical Society and IOP Publishing Ltd

veal a quite different density of states (DOS) near the Fermi level ($E_F$) of $NaMn_6Bi_5$ compared with those of other $AMn_6Bi_5$ ($A$ = K, Rb, and Cs). These results show that $NaMn_6Bi_5$ is a more promising candidate to explore the interplay of magnetism and superconductivity and other possible exotic properties.

*Experimental—Single Crystal Growth.* $NaMn_6Bi_5$ single crystals were grown by a high-temperature solution method modified from that reported in our former work.[25] Na chunk (99.75%, Alfa Aesar), Mn powder (99.95%, Alfa Aesar), and Bi granules (99.999%, Sinopharm) were mixed using a molar ratio of Na:Mn:Bi = 0.5 : 4 : 8 in a fritted alumina crucible set (Canfield crucible set)[28] and sealed in a fused-silica ampoule at vacuum. The ampoule was heated to 1073 K over 15 h, held at the temperature for 24 h, and then slowly cooled down to 673 K at a rate of 2 K/h. At 673 K, the single crystals with size up to 5 mm × 0.5 mm × 0.5 mm were separated from the remaining liquid by centrifuging the ampoule. The obtained single crystals are shiny-silver needles and air-sensitive, so all manipulations and specimen preparation for structure characterization and property measurements were handled in an argon-filled glovebox. In addition, $CsMn_6Bi_5$ single crystals were also grown using the similar method.

*Structure Characterization and Composition Analysis.* X-ray diffraction data were obtained using a PANalytical X'Pert PRO diffractometer (Cu $K_\alpha$ radiation, $\lambda$ = 1.54178 Å) operated at 40 kV voltage and 40 mA current with a graphite monochromator in a reflection mode ($2\theta = 5°$–$80°$ with steps of 0.017°). Indexing and Rietveld refinement were performed using the DICVOL91 and FULLPROF programs.[29] Single crystal x-ray diffraction (SCXRD) data were collected using a Bruker D8 VENTURE with Mo $K_\alpha$ radiation ($\lambda$ = 0.71073 Å) at 300 K. The structure was solved using a direct method and refined with the Olex2 package.[30] The morphology and analyses of elements were characterized using a scanning electron microscope (SEM, Hitachi S-4800) equipped with an electron microprobe analyzer for semiquantitative elemental analysis in energy-dispersive spectroscopy (EDS) mode, combing with the inductively coupled plasma-atomic emission spectrometer (ICP-AES, Teledyne Leeman Laboratories Prodigy 7). Five spots in different areas were measured on one crystal using EDS, and the ICP-AES measurement was performed on two pieces of single crystals separately. The crystal structure and chemical composition of $CsMn_6Bi_5$ single crystal have also been determined.

*Physical Property Measurements.* The magnetic susceptibility, resistivity, and heat capacity measurements were carried out using a physical property measurement system (PPMS, Quantum Design). Magnetic susceptibility was measured under a small magnetic field (0.1 T) parallel ($H$//rod) and perpendicular ($H\perp$rod) to the rod ([010] direction) using the zero-field-cooling (ZFC) and field-cooling (FC) protocols as reported in $RbMn_6Bi_5$.[25] For larger fields at 1, 2, 3, 5, and 7 T, only magnetic susceptibility in FC protocol was measured. Isothermal magnetization curves at 5, 10, 40, 50, 100, and 300 K were measured under the magnetic field up to 7 T parallel and perpendicular to the rod ([010] direction). The resistivity was measured using the standard four-probe configuration with the applied current (about 2 mA) parallel ($I$//rod) or perpendicular ($I\perp$rod) to the rod ([010] direction). Heat capacity measurement was carried out below 200 K. To protect the samples from air and moisture, thin film of n-type grease was spread to cover the sample for heat capacity measurement.

*First-Principles Calculations.* The first-principles calculations were carried out with the projector augmented wave method as implemented in the Vienna *ab initio* simulation package (VASP).[31,32] The generalized gradient approximation[33] of the Perdew–Burke–Ernzerhof[34] type was adopted for the exchange-correlation function. The cutoff energy of the plane-wave basis was 500 eV and the energy convergence standard was set to $10^{-8}$ eV. The 3×11×4 Monkhorst–Pack $K$-point mesh was employed for the Brillouin zone sampling of the 1 × 1 × 1 unit cell containing 48 atoms. Since Bi is a quite heavy element, spin-orbit coupling (SOC) effect is taken into account.

*Results and Discussion.—Crystal Structure.* As shown in the inset of Fig. 1(a), the as-grown single crystals of $NaMn_6Bi_5$ are needle-like rods with shiny metal luster, indicating a clear quasi-one-dimensional feature. The x-ray diffraction pattern of an as-grown crystal is plotted in Fig. 1(a) with a strong preferential orientation of (00$l$) ($l$ = integer) reflections. Based on the position (∼8.2°) of (001) diffraction peak, the distance between corresponding structural units is determined to be 12.6 Å, which is close to the lattice parameter $c$ as reported in $KMn_6Bi_5$ and $RbMn_6Bi_5$.[24,25] Elemental mapping of $NaMn_6Bi_5$ [Fig. 1(b)] confirms the homogeneous distribution of Na, Mn, and Bi. According to EDS (Fig. S1 in the Supplementary Material), the molar ratio is close to Na:Mn:Bi = 1 : 6.37(2) : 5.22(3), whereas ICP-AES indicates a molar ratio of Na:Mn:Bi = 1.008(2) : 6.000(1) : 4.967(2). Considering its quasi-one-dimensional feature, we tried to mechanically exfoliate the crystals using the scotch-tape method and obtained $NaMn_6Bi_5$ wires with diameter down to 528 nm (Fig. S1), showing possibilities in applications.

The determined crystal structure based on the SCXRD data is shown in Figs. 1(c) and 1(d). $NaMn_6Bi_5$ crystallizes in a monoclinic space group (Table S1) $C2/m$ (No. 12) with $a$ = 22.3894(12) Å, $b$ = 4.5872(3) Å, $c$ = 12.6398(7) Å, $\alpha = \gamma = 90°$, and

$\beta = 123.0602(15)°$. As shown in Fig. 1(c), $NaMn_6Bi_5$ shares a similar quasi-one-dimensional structure motif with that of $KMn_6Bi_5$[24] and $RbMn_6Bi_5$,[25] featuring $[Mn_6Bi_5]^-$ columns extending along the [010] direction, which is surrounded by $Na^+$ acting as separators. The $[Mn_6Bi_5]^-$ column consists of the $Mn_5$ tunnel built by Mn$i$ ($i = 1$–5) with an inner one-dimensional Mn6–Mn6 atomic chain and the outmost $Bi_5$ tunnel.

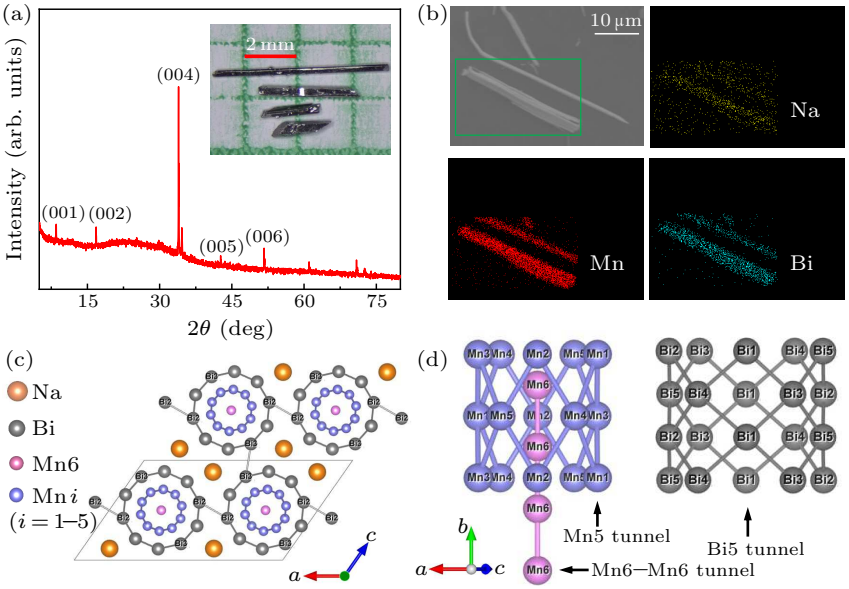


**Fig. 1.** (a) X-ray diffraction pattern of an as-grown $NaMn_6Bi_5$ single crystal, showing (00$l$) reflections. The inset is the optical photograph of $NaMn_6Bi_5$ single crystals. (b) SEM image of $NaMn_6Bi_5$ and elemental mapping. (c) Crystal structure of $NaMn_6Bi_5$ viewed along $b$ axis with inter-column bonds Bi2–Bi2 and Bi3–Bi3 labeled. (d) Crystal structure of $Mn_5$ tunnel with one-dimensional Mn6–Mn6 chain at the center and $Bi_5$ tunnel viewed perpendicular to $ab$ plane.

The lattice parameters and typical bond lengths of $AMn_6Bi_5$ ($A$ = Na, K, Rb, and Cs) are summarized in Table 1. With the increasing radius from $Na^+$ (~102 pm) to $K^+$ (~138 pm), then to $Rb^+$ (~152 pm), and finally to $Cs^+$ (~167 pm), the lattice parameters $a$, $c$, and $\beta$ all increase monotonically. Compared with $RbMn_6Bi_5$, $NaMn_6Bi_5$ shows shrinkage of $a$ and $c$ as large as 3.85% and 7.27%, respectively, whereas that of $b$ is only 0.74%. Such differences can be interpreted by the strong bonds of Mn–Mn and Bi–Bi along $b$ axis and the much weaker inter-column Na–Bi bonds. The varying $\beta$ suggests potential glides of $[Mn_6Bi_5]^-$ columns along $a$ or $c$ axis, which means that $AMn_6Bi_5$ ($A$ = Na, K, Rb, and Cs) could be tuned using stress or pressure. Among all the intra-column bonds, two typical intra-column bond lengths monotonically increase with increasing cation radius, from 3.5076(15) Å (Na) to 3.5392(7) Å (Cs) for Bi2–Bi4, and from 3.428(3) Å (Na) to 3.5704(14) Å (Cs) for Bi3–Bi5, respectively. By contrast, the other three typical intra-column bond lengths show decreasing tendency from 3.5376(18) Å (Na) to 3.4912(11) Å (Cs) for Bi2–Bi5, from 3.562(3) Å (Na) to 3.4714(13) Å (Cs) for Bi1–Bi3, and 3.6115(8) Å (K) to 3.6015(10) Å (Cs) for Bi2–Bi4 but with an anomaly (3.596(3) Å) for $NaMn_6Bi_5$. Moreover, the inter-column bond (Bi3–Bi3) monotonically increases from 3.540(4) Å (Na) to 3.7698(18) Å (Cs) as cation radius increases, whereas another inter-column bond (Bi2–Bi2) shows an anomaly for $NaMn_6Bi_5$, with the relation 3.5688(13) Å (K) <3.606(3) Å (Rb) <3.628(4) Å (Na) <3.6812(18) Å (Cs). These abnormal Bi–Bi bond lengths for $NaMn_6Bi_5$ should be correlated with its unusual properties (see below).

**Table 1.** Lattice parameters and typical bond lengths of $AMn_6Bi_5$ ($A$ = Na, K, Rb, and Cs).

| $A$ | Na | K[24] | Rb[25] | Cs |
|---|---|---|---|---|
| Radius (pm) | 102 | 138 | 152 | 167 |
| $a$ (Å) | 22.3894(12) | 22.994(2) | 23.286(5) | 23.6338(14) |
| $b$ (Å) | 4.5872(3) | 4.6128(3) | 4.6215(9) | 4.6189(3) |
| $c$ (Å) | 12.6398(7) | 13.3830(13) | 13.631(3) | 13.8948(8) |
| $\alpha, \gamma$ (deg) | 90 | 90 | 90 | 90 |
| $\beta$ (deg) | 123.0602(15) | 124.578(6) | 125.00(3) | 125.447(2) |
| Bi2–Bi4 (Å) | 3.5076(15) | 3.5289(6) | 3.5363(15) | 3.5392(7) |
| Bi3–Bi5 (Å) | 3.428(3) | 3.5165(9) | 3.548(2) | 3.5704(14) |
| Bi2–Bi5 (Å) | 3.5376(18) | 3.5309(7) | 3.5165(17) | 3.4912(11) |
| Bi1–Bi3 (Å) | 3.562(3) | 3.5138(10) | 3.493(2) | 3.4714(13) |
| Bi1–Bi4 (Å) | 3.596(3) | 3.6115(8) | 3.6111(18) | 3.6015(10) |
| Bi3–Bi3 (Å) | 3.540(4) | 3.6518(14) | 3.703(4) | 3.7698(18) |
| Bi2–Bi2 (Å) | 3.628(4) | 3.5688(13) | 3.606(3) | 3.6812(18) |

*Magnetic Property.* Figures 2(a) and 2(b) show the ZFC and FC magnetic susceptibility of $NaMn_6Bi_5$ single crystals under 0.1 T with $H$//rod and $H\perp$rod ([010] direction), respectively. The insets in Figs. 2(a) and 2(b) show the $d\chi T/dT$ curves, donating the magnetic transition temperatures. For $H$//rod, the ZFC

and FC curves coincide with each other in the entire measured temperature range (2–120 K), showing two AFM-like transitions at 45.3 K and 50.9 K. For $H\perp$rod, a small deviation is observed in the AFM-like transition temperatures (black arrows), with a small kink emerging at 85.7 K (Fig. S2). The newly emerged kink and the bifurcation of ZFC and FC curves can be attributed to the magnetic anisotropy.[35]

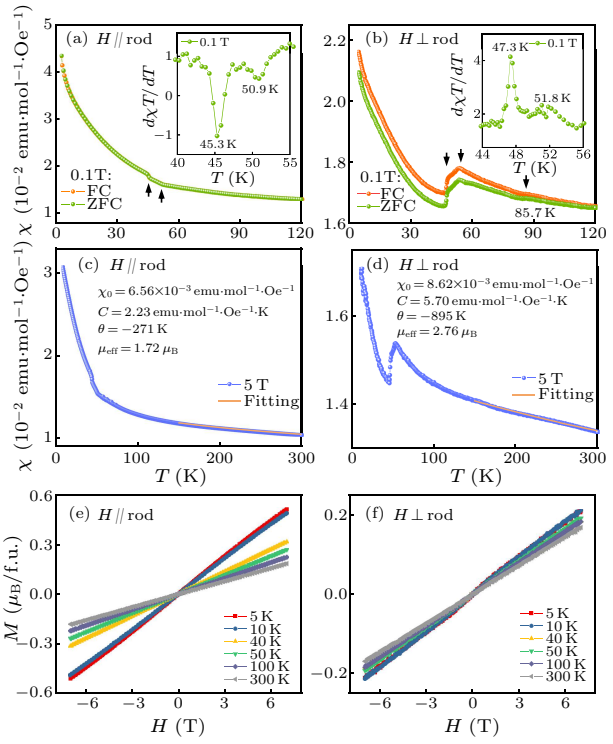


**Fig. 2.** ZFC and FC magnetic susceptibility of $NaMn_6Bi_5$ single crystals under 0.1 T for (a) $H//$rod and (b) $H\perp$rod ([010] direction). The insets are the corresponding $d\chi T/dT$ curves. Temperature dependent magnetic susceptibility of $NaMn_6Bi_5$ single crystals under 5 T for (c) $H//$rod and (d) $H\perp$rod and the corresponding Curie–Weiss fittings from 150 K to 300 K. Field dependent magnetizations for (e) $H//$rod and (f) $H\perp$rod at different temperatures.

By fitting the magnetic susceptibility under 5 T in a higher temperature range (150–300 K) using the Curie–Weiss law $\chi = \chi_0 + C/(T-\theta)$, where $\chi_0$ is the temperature-independent contribution including the diamagnetic contribution of the orbital magnetic moment and the Pauli paramagnetic contribution of conduction electron, $C$ the Curie constant, and $\theta$ the Curie temperature.[36] The fitted values are $\chi_0 = 6.56\times10^{-3}$ emu·mol$^{-1}$·Oe$^{-1}$, $\theta = -271$ K, and $C = 2.23$ emu·mol$^{-1}$·Oe$^{-1}$·K for $H//$rod, whereas $\chi_0 = 8.62\times10^{-3}$ emu·mol$^{-1}$·Oe$^{-1}$, $\theta = -895$ K, and $C = 5.70$ emu·mol$^{-1}$·Oe$^{-1}$·K for $H\perp$rod. Negative $\theta$ indicates that the interactions in both directions are of AFM character. The frustration factors $|\theta/T_N|$[37] are calculated to be ∼6 for $H//$rod and ∼19 for $H\perp$rod, indicating an anisotropic frustration. This may be attributed to the quite large magnetic anisotropy resulted from the geometry of the quasi-one-dimensional motif. The effective moment can be derived following the equation $\mu_{\rm eff} = \sqrt{8C/n}$, where $n$ is the number of magnetic atoms. For $NaMn_6Bi_5$, the effective moment is $\mu_{\rm eff} \sim 1.72\mu_B$/Mn for $H//$rod and $\mu_{\rm eff} \sim 2.76\mu_B$/Mn for $H\perp$rod, respectively. As discussed in $RbMn_6Bi_5$,[25] these values fall in the range of the spin-only magnetic moment of low-spin $t_{2g}^{4.67}$ ($1.38\mu_B$) and high-spin $t_{2g}^{3}e_g^{1.67}$ ($5.48\mu_B$) of octahedrally coordinated $d^{4.67}$, corresponding to the Zintl phase[38] with an average oxidation state of $Mn^{2.33+}$. The magnetic anisotropy in $NaMn_6Bi_5$ is larger than that of $KMn_6Bi_5$, which may be attributed to the effect of cation radius.

The magnetization of $NaMn_6Bi_5$ under magnetic fields parallel and perpendicular to the rod ([010] direction) are shown in Figs. 2(e) and 2(f), respectively. All magnetization curves increase almost linearly with magnetic field ranging from 5 K to 300 K and remain unsaturated up to 7 T with no hysteresis loop in both directions. The absence of hysteresis in $M$–$H$ curves confirms the dominant AFM interaction at low temperatures, as same as in $KMn_6Bi_5$[24] and $RbMn_6Bi_5$.[25] By increasing the magnetic field from 1 T to 7 T for $H//$rod, the two AFM-like transition temperatures hardly change (Fig. S2), showing that the Mn moments in $NaMn_6Bi_5$ have a large saturation magnetic field. Compared with the transition temperatures of $KMn_6Bi_5$ (∼75 K)[24] and $RbMn_6Bi_5$ (∼80 K),[25] the AFM-like transition temperature (50.9 K) is largely suppressed in $NaMn_6Bi_5$. Moreover, a possible new AFM-like transition emerges at 45.3 K. As predicted in $RbMn_6Bi_5$, the moments of Mn at the center couple with the moments of Mn at the pentagon, inducing a helical magnetic order with one magnetic transition temperature.[25] Once these two kinds of moments are decoupled, multiple transitions are expected. The observed lower AFM-like transition temperatures, more AFM-like transitions, and the small kink at higher temperature may be the hint of such decoupling, whereas the underlying mechanism still remains uncovered. Further investigation, such as neutron diffraction or high-resolution magnetic torque measurement, will be needed to characterize the possible multiple magnetic structures of $NaMn_6Bi_5$. More importantly, the lower AFM-like transition temperature makes $NaMn_6Bi_5$ a more promising candidate to explore Mn-based superconductor by chemical doping or applying physical pressure.

*Resistivity.* With $I//$rod, the resistivity of $NaMn_6Bi_5$ decreases with decreasing temperature, showing a metallic-like behavior with a small kink at 87.6 K (Fig. S3) and an obvious anomaly around 50 K [Fig. 3(a)]. From the first derivative ($d\rho/dT$) curve, two transition temperatures at 47.2 K and 53.3 K can

be extracted and coincide with AFM-like transition temperatures observed in the magnetic susceptibility, which are sample-independent (Fig. S3). The room-temperature resistivity for $NaMn_6Bi_5$ is estimated to be 0.207 mΩ·cm in the [010] direction, smaller than the maximum value (1 mΩ·cm) determined by the Mott–Ioffe–Regel limit.[39] The residual resistivity ratio RRR = $\rho(300\,\mathrm{K})/\rho(2\,\mathrm{K})$ = 6.5 indicates that the crystalline quality of $NaMn_6Bi_5$ is good. Above 55 K, the resistivity can be fitted [red line in Fig. 3(a)] using the formula $\frac{1}{\rho(T)} = \frac{1}{\rho_{\mathrm{sat}}} + \frac{1}{\rho_{\mathrm{ideal}}}$, where $\rho_{\mathrm{sat}}$ represents the saturation resistivity, $\rho_{\mathrm{ideal}}$ is the ideal resistivity that satisfies the Boltzmann equation; $\rho_{\mathrm{ideal}}$ is proportional to the temperature in the higher temperature region and can be described by $\rho_{\mathrm{ideal}} = \rho_{\mathrm{r}} + aT$.[39] The fitting yields $\rho_{\mathrm{sat}}$ = 0.24 mΩ·cm, $\rho_{\mathrm{r}}$ = 0.33 mΩ·cm, and $a = 4.4\times10^{-3}$ mΩ·cm·K$^{-1}$. As shown in Fig. 4(c), the resistivity can be well fitted using $\rho = \rho_0 + AT^{\alpha}$ below 25 K, with fitted parameters $\rho_0$ = 0.0295 mΩ·cm, $A = 7.47\times10^{-4}$ mΩ·cm·K$^{-1.39}$, and $\alpha$ = 1.39. The value of power $\alpha$ deviates largely from 2, suggesting a non-Fermi liquid behavior of $NaMn_6Bi_5$ at low temperatures, which is quite different from the Fermi liquid behavior reported in both $KMn_6Bi_5$ ($\alpha \sim 2$)[24] and $RbMn_6Bi_5$ ($\alpha = 1.9$).[25]

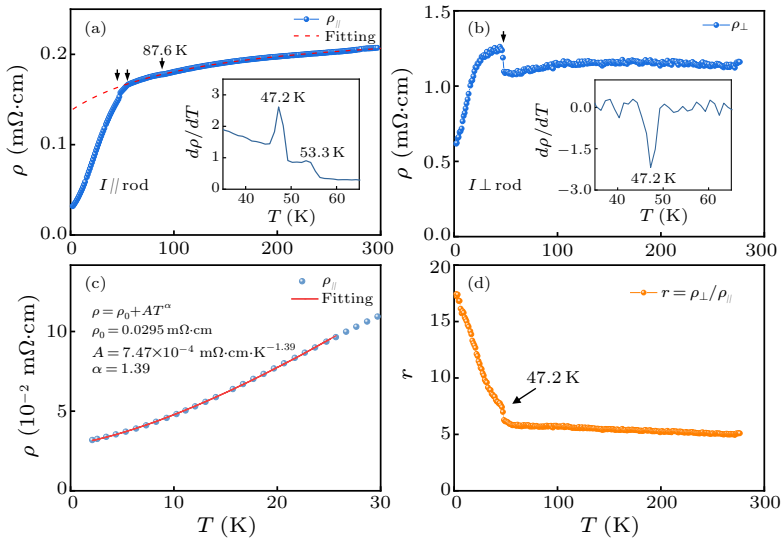


**Fig. 3.** Temperature-dependent resistivity $\rho(T)$ for $NaMn_6Bi_5$ single crystal measured with (a) $I$//rod and (b) $I\perp$rod ([010] direction). The insets are the first derivative in the temperature range 35–65 K. (c) The enlarged low-temperature resistivity with $I$//rod. (d) Temperature-dependent anisotropic resistivity ratio for $NaMn_6Bi_5$ single crystal.

In comparison, temperature-dependent resistivity with $I\perp$rod only shows a jump around 47.2 K [Fig. 3(b)]. The transition at 53.3 K and the small kink around 87.6 K are not observed, which is probably too weak to be detected in the experimental data with a larger noise. Below the jump, the resistivity begins to decrease with the decreasing temperature. Unlike the hump coming from the dimensional crossover of electrons in low-dimensional materials observed in $KMn_6Bi_5$ and $RbMn_6Bi_5$,[24,25,40] the resistivity jump is probably due to the AFM transitions which reduce the carrier concentrations and thus increase the resistivity. The anisotropic resistivity ratio, donated as $r = \rho_{\perp}/\rho_{||}$, increases with decreasing temperature and sharply increases below the AFM-like transition temperature [Fig. 3(d)]. The value of anisotropic resistivity ratio is about 17 at 2 K, comparable to that of $KMn_6Bi_5$ (∼20)[24] but much smaller than that of $RbMn_6Bi_5$ (∼240).[25]

*Specific Heat Capacity.* Temperature-dependent specific heat capacity for $NaMn_6Bi_5$ single crystal measured from 2 K to 200 K is shown in Fig. 4(a), which exhibits two peaks at 45.9 K and 52.2 K and a small kink at 85.0 K. These temperatures are close to the transition temperatures of magnetic susceptibility and resistivity, which are sample-independent (Fig. S4) and reversible for cooling down and warming up [Fig. 4(b)]. The specific heat capacity exceeds the Dulong–Petit limit ($3NR \sim 300\,\mathrm{J\cdot mol^{-1}\cdot K^{-1}}$, yellow dashed line) at higher temperature, which is also attributed to more prominent phonon contribution at higher temperature of n-type grease used for protecting the sample.[24,25] For $NaMn_6Bi_5$, both jumps $\Delta C \sim 28\,\mathrm{J\cdot mol^{-1}\cdot K^{-1}}$ and $11\,\mathrm{J\cdot mol^{-1}\cdot K^{-1}}$ are much smaller than that of $KMn_6Bi_5$ ($\Delta C \sim 180\,\mathrm{J\cdot mol^{-1}\cdot K^{-1}}$) and $RbMn_6Bi_5$ ($\Delta C \sim 175\,\mathrm{J\cdot mol^{-1}\cdot K^{-1}}$). We then fit the low-temperature (2–5 K) specific heat capacity with the Debye model $C = \gamma T + \beta T^3$, where $\gamma T$ represents the contribution from the electron, $\beta T^3$ represents the contribution of the lattice. Because of the insulating character of n-type grease, the Sommerfeld coefficient

correlated with the electron contribution will not be affected at low temperature. The Sommerfeld coefficient $\gamma$ proportional to the DOS [$\gamma \propto g(E_F)$][41] at $E_F$ is determined to be 139.13 mJ·K$^{-2}$ per formula [23.2 mJ·K$^{-2}$·(mol-Mn)$^{-1}$], much larger (3–5 times) than that of $KMn_6Bi_5$ (39.0 mJ·K$^{-2}$ per formula)[24] and $RbMn_6Bi_5$ (28.2 mJ·K$^{-2}$ per formula).[25] This indicates the decreasing trend of DOS at $E_F$ by increasing the cation radius from Na to Rb, which is also held for other quasi-one-dimensional materials such as $A_2Cr_3As_3$ ($A$ = K, Rb, and Cs)[16–18] with the underlying mechanism unknown.

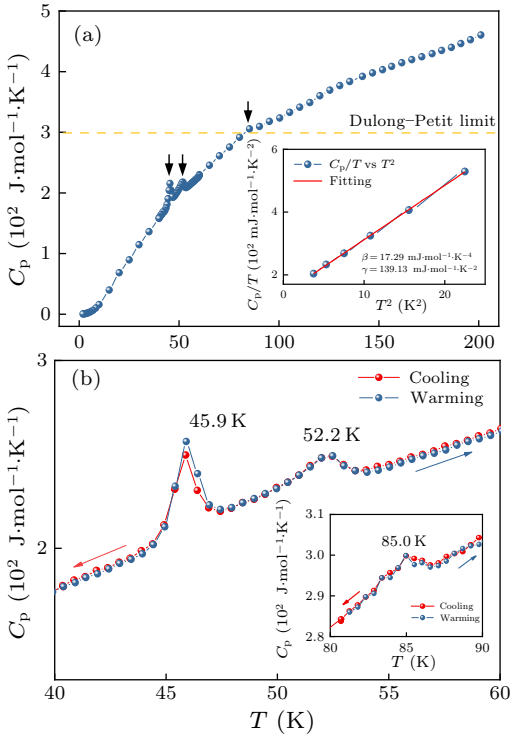


**Fig. 4.** (a) Temperature-dependent specific heat capacity for $NaMn_6Bi_5$ single crystal. The inset shows the $C_p/T$ versus $T^2$, the red solid line is the linear fit using the Debye model. (b) The enlarged specific heat capacity around 50 K and 85 K for cooling down and warming up.

*Density of States.* We then tried to understand the effect of structure anomaly in $NaMn_6Bi_5$ and the origin of its different magnetic transitions, non-Fermi liquid behavior, and much enhanced Sommerfeld coefficient by calculating DOS near $E_F$ for $AMn_6Bi_5$ ($A$ = Na, K, Rb, and Cs) using first-principles calculations. As shown in Fig. 5, all $AMn_6Bi_5$ ($A$ = Na, K, Rb, and Cs) compounds have nonzero DOS at $E_F$, corresponding well with the observed metallic-like behavior in resistivity. Compared with other $AMn_6Bi_5$ ($A$ = K, Rb, and Cs) compounds, $NaMn_6Bi_5$ shows a quite different DOS near $E_F$, which may correspond to those different characteristics. A peak of DOS exists at $E_F$ for $KMn_6Bi_5$ and becomes higher for $RbMn_6Bi_5$ and broader for $CsMn_6Bi_5$, whereas a dip (blue arrow) is observed for $NaMn_6Bi_5$. Below $E_F$, a high peak (red arrow) is observed, showing a dense distribution of occupied electrons near $E_F$ for $NaMn_6Bi_5$. Considering the classical relation between DOS [$g(E)$] and effective mass $m^*$ (see Ref. [41]): $g(E) = \frac{1}{2\pi^2}\left(\frac{2m^*}{\hbar^2}\right)^{3/2}E^{1/2}$, the denser distribution of DOS corresponds to a larger effective mass of $NaMn_6Bi_5$, which should be responsible for the much enhanced Sommerfeld coefficient. More investigations should be carried out to resolve why larger effective mass appears in quasi-one-dimensional materials with a smaller alkali metal.

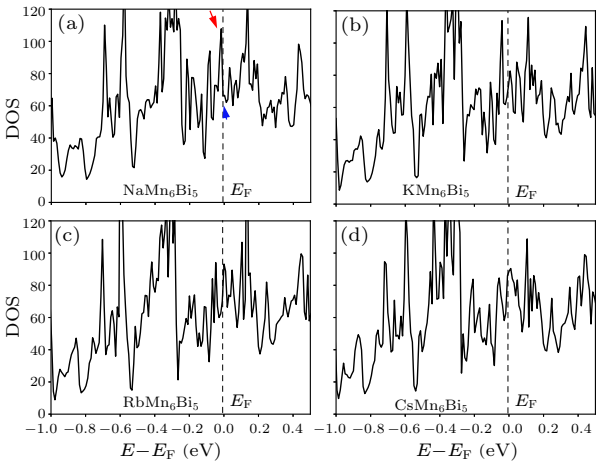


**Fig. 5.** DOS with SOC near $E_F$ (dashed lines) from −1 eV to 0.5 eV for (a) $NaMn_6Bi_5$, (b) $KMn_6Bi_5$, (c) $RbMn_6Bi_5$, and (d) $CsMn_6Bi_5$. Red and blue arrows donate the difference of DOS for $NaMn_6Bi_5$ around $E_F$ compared with other $AMn_6Bi_5$ ($A$ = K, Rb, and Cs) compounds.

In conclusion, a new quasi-one-dimensional superconductor parent compound $NaMn_6Bi_5$ has been discovered. Compared with other $AMn_6Bi_5$ ($A$ = K, Rb, and Cs), $NaMn_6Bi_5$ has abnormal Bi–Bi bond lengths. The structure anomaly may result in the two possibly decoupled AFM-like transitions at 47.3 K and 51.8 K observed in magnetic susceptibility, resistivity, and heat capacity measurements. Anisotropic resistivity, non-Fermi liquid behavior, and much enhanced Sommerfeld coefficient are observed, which may be attributed to the enhanced DOS near $E_F$ compared with other $AMn_6Bi_5$ ($A$ = K, Rb, and Cs) compounds. The decoupled AFM-like transitions and lower AFM-like transition temperatures make $NaMn_6Bi_5$ a more promising platform for exploring the exchange-coupling interaction and interplay of magnetism and superconductivity. Chemical doping and physical pressure should be the effective means to induce superconductivity within such quasi-one-dimensional materials with possible helical magnetic order.

*Supplementary Material.* Table S1 compares the crystal structures of $NaMn_6Bi_5$ and $CsMn_6Bi_5$. Figure S1 displays the quasi-one-dimensional feature of $NaMn_6Bi_5$. Figure S2 shows the magnetic susceptibil-

ity of $NaMn_6Bi_5$ single crystal under various magnetic field. Figures S3–S4 are temperature-dependent resistivity and specific heat capacity of other $NaMn_6Bi_5$ single crystals.

*Acknowledgements.* This work was partially supported by the National Key Research and Development Program of China (Grant Nos. 2017YFA0302902 and 2018YFE0202600), the National Natural Science Foundation of China (Grant No. 51832010 and 11888101), and the Key Research Program of Frontier Sciences, Chinese Academy of Sciences (Grant No. QYZDJ-SSW-SLH013).

## References

[1] Bednorz J G and Müller K A 1986 *Z. Phys. B: Condens. Matter* **64** 189
[2] Zhao Z X, Chen L Q, Cui C G, Huang Y Z, Liu J X, Chen G H, Li S L, Guo S Q and He Y Y 1987 *Sci. Bull.* **32** 522
[3] Lee P A, Nagaosa N and Wen X G 2006 *Rev. Mod. Phys.* **78** 17
[4] Chen L H, Wang D, Zhou Y and Wang Q H 2020 *Chin. Phys. Lett.* **37** 017403
[5] Kamihara Y, Hiramatsu H, Hirano M, Kawamura R, Yanagi H, Kamiya T and Hosono H 2006 *J. Am. Chem. Soc.* **128** 10012
[6] Kamihara Y, Watanabe T, Hirano M and Hosono H 2008 *J. Am. Chem. Soc.* **130** 3296
[7] Chen X H, Wu T, Wu G, Liu R H, Chen H and Fang D F 2008 *Nature* **453** 761
[8] Steglich F, Aarts J, Bredl C D, Lieke W, Meschede D, Franz W and Schäfer H 1979 *Phys. Rev. Lett.* **43** 1892
[9] Stewart G R 1984 *Rev. Mod. Phys.* **56** 755
[10] Alireza P L, Ko Y C, Gillett J, Petrone C M, Cole J M, Lonzarich G G and Sebastian S E 2009 *J. Phys.: Conden. Matter* **21** 012208
[11] Akbari A, Eremin I and Thalmeier P 2011 *Phys. Rev. B* **84** 134513
[12] Marty K, Christianson A D, Wang C H, Matsuda M, Cao H, VanBebber L H, Zarestky J L, Singh D J, Sefat A S and Lumsden M D 2011 *Phys. Rev. B* **83** 060509
[13] Chen L, Cao C, Chen H X, Guo J G, Ma J, Hu J P and Wang G 2021 *Phys. Rev. B* **103** 134509
[14] Gao Q, Zhao L, Hu C, Yan H T, Chen H, Cai Y Q, Li C, Ai P, Liu J, Huang J W, Rong H T, Song C Y, Yin C H, Wang Q Y, Huang Y, Liu G D, Xu Z Y and Zhou X J 2020 *Chin. Phys. Lett.* **37** 087402
[15] Wu W, Cheng J G, Matsubayashi K, Kong P P, Lin F K, Jin C Q, Wang N L, Uwatoko Y and Luo J L 2014 *Nat. Commun.* **5** 5508
[16] Bao J K, Liu J Y, Ma C W, Meng Z H, Tang Z T, Sun Y L, Zhai H F, Jiang H, Bai H, Feng C M, Xu Z A and Cao G H 2015 *Phys. Rev. X* **5** 011013
[17] Tang Z T, Bao J K, Liu Y, Sun Y L, Ablimit A, Zhai H F, Jiang H, Feng C M, Xu Z A and Cao G H 2015 *Phys. Rev. B* **91** 020506
[18] Tang Z T, Bao J K, Wang Z, Bai H, Jiang H, Liu Y, Zhai H F, Feng C M, Xu Z A and Cao G H 2015 *Sci. Chin. Mater.* **58** 16
[19] Dahal A, Gunasekera J and Singh D K 2017 *Phys. Status Solidi RRL* **11** 1700211
[20] Cheng J G, Matsubayashi K, Wu W, Sun J P, Lin F K, Luo J L and Uwatoko Y 2015 *Phys. Rev. Lett.* **114** 117001
[21] Matsuda M, Ye F, Dissanayake S E, Cheng J G, Chi S, Ma J, Zhou H D, Yan J Q, Kasamatsu S, Sugino O, Kato T, Matsubayashi K, Okada T and Uwatoko Y 2016 *Phys. Rev. B* **93** 100405(R)
[22] Li D F, Lee K, Wang B Y, Osada M, Crossley S, Lee H R, Cui Y, Hikita Y and Hwang H Y 2019 *Nature* **572** 624
[23] Gu Q Q and Wen H H 2022 *Innovation* **3** 100202
[24] Bao J K, Tang Z T, Jun H J, Liu J Y, Liu Y, Li L, Li Y K, Xu Z A, Feng C M, Chen H J, Chung D Y, Dravid V P, Cao G H and Kanatzidis M G 2018 *J. Am. Chem. Soc.* **140** 4391
[25] Chen L, Zhao L L, Qiu X L, Zhang Q H, Liu K, Lin Q S and Wang G 2021 *Inorg. Chem.* **60** 12941
[26] Liu Z Y, Dong Q X, Yang P T, Shan P F, Wang B S, Sun J P, Uwatoko Y, Chen G F, Dong X L, Zhao Z X and Cheng J G 2022 arXiv:2201.06053 [cond-mat.supr-con]
[27] Yang P T, Dong Q X, Shan P F, Liu Z Y, Sun J P, Dun Z L, Uwatoko Y, Chen G F, Wang B S and Cheng J G 2022 arXiv:2201.13336 [cond-mat.supr-con]
[28] Canfield P C, Kong T, Kaluarachchi U S and Jo N H 2016 *Philos. Mag.* **96** 84
[29] Rodríguez-Carvajal J 2001 *FullProf* (CEA/Saclay, France)
[30] Dolomanov O V, Bourhis L J, Gildea R J, Howard J A and Puschmann H 2009 *J. Appl. Crystallogr.* **42** 339
[31] Kresse G and Hafner J 1993 *Phys. Rev. B* **47** 558
[32] Kresse G and Furthmuller J 1996 *Phys. Rev. B* **54** 11169
[33] Perdew J P, Burke K and Ernzerhof M 1997 *Phys. Rev. Lett.* **78** 1396
[34] Kresse G and Furthmuller J 1996 *Comput. Mater. Sci.* **6** 15
[35] Wang W J, Sun R, He S J, Jia Z Y, Su C L, Li Y and Wang Z C 2021 *2D Mater.* **8** 015027
[36] Johnston D C 2010 *Adv. Phys.* **59** 803
[37] Greedan J E 2001 *J. Mater. Chem.* **11** 37
[38] Nesper R 2014 *Z. Anorg. Allg. Chem.* **640** 2639
[39] Gunnarsson O, Calandra M and Han J E 2003 *Rev. Mod. Phys.* **75** 1085
[40] Valla T, Johnson P D, Yusof Z, Wells B, Li Q, Loureiro S M, Cava R J, Mikami M, Mori Y, Yoshimura M and Sasaki T 2002 *Nature* **417** 627
[41] Ashcroft N W and Mermin N D 1976 *Solid State Physics* (Philadelphia, PA: Saunders College)

# Supplementary Material for "A New Superconductor Parent Compound $NaMn_6Bi_5$ with Quasi-One-Dimensional Structure and Lower Antiferromagnetic-Like Transition Temperatures"

Ying Zhou(周颖)[1, 2, #], Long Chen(陈龙)[1, 2, #], Gang Wang(王刚)[1, 2, 3, *], Yu-Xin Wang(王郁欣)[1, 2], Zhi-Chuan Wang(王志川)[1, 2], Cong-Cong Chai(柴聪聪)[1, 2], Zhong-Nan Guo(郭中楠)[4], Jiang-Ping Hu(胡江平)[1, 2, 3, *], and Xiao-Long Chen(陈小龙)[1, 2, 3, *]

[1] Beijing National Laboratory for Condensed Matter Physics, Institute of Physics, Chinese Academy of Sciences, Beijing 100190, China

[2] University of Chinese Academy of Sciences, Beijing 100049, China

[3] Songshan Lake Materials Laboratory, Dongguan, Guangdong 523808, China

[4] Department of Chemistry, School of Chemistry and Biological Engineering, University of Science and Technology Beijing, Beijing 100083, China

[#] These authors contributed equally to this work.

[*]Corresponding author. Email: gangwang@iphy.ac.cn; jphu@iphy.ac.cn; xlchen@iphy.ac.cn.

**Table S1.** Crystal structures of $NaMn_6Bi_5$ and $CsMn_6Bi_5$ obtained by structural refinement from single crystal X-ray diffraction data.

| Empirical formula | $NaMn_6Bi_5$ | $CsMn_6Bi_5$ |
|---|---|---|
| Formula weight | 1397.53 g/mol | 1507.43 g/mol |
| Space group / Z | *C*2/*m* (No. 12) /4 | *C*2/*m* (No. 12) /4 |
| Unit cell dimensions | $a$ = 22.3894(12) Å | $a$ = 23.6338(14) Å |
| | $b$ = 4.5872(3) Å | $b$ = 4.6189(3) Å |
| | $c$ = 12.6398(7) Å | $c$ = 13.8948 (8) Å |
| | $\alpha = \gamma$ = 90 ° | $\alpha = \gamma$ = 90 ° |
| | $\beta$ = 123.0602(15) ° | $\beta$ = 125.447(2) ° |
| Volume / $d_{cal}$ | 1087.99(11) Å$^3$ / 8.532 g/cm$^3$ | 1235.6(5) Å$^3$ / 8.711 g/cm$^3$ |
| Reflections collected/R(int) | 6072 / 0.0824 | 6427 / 0.079 |
| Data / restraints / parameters | 1517 / 0 / 73 | 1278 / 0 / 73 |
| Final R indices [I > 2sigma(I)] | $R_1$ = 0.1327, $wR_2$ = 0.3581 | $R_1$ = 0.0512, $wR_2$ = 0.0565 |
| *R* indices (all data) | $R_1$ = 0.1344, $wR_2$ = 0.3613 | $R_1$ = 0.0595, $wR_2$ = 0.0603 |
| Largest diff. peak and hole | 21.337 and -22.760 e.Å$^{-3}$ | 1.010 and -2.132 e.Å$^{-3}$ |

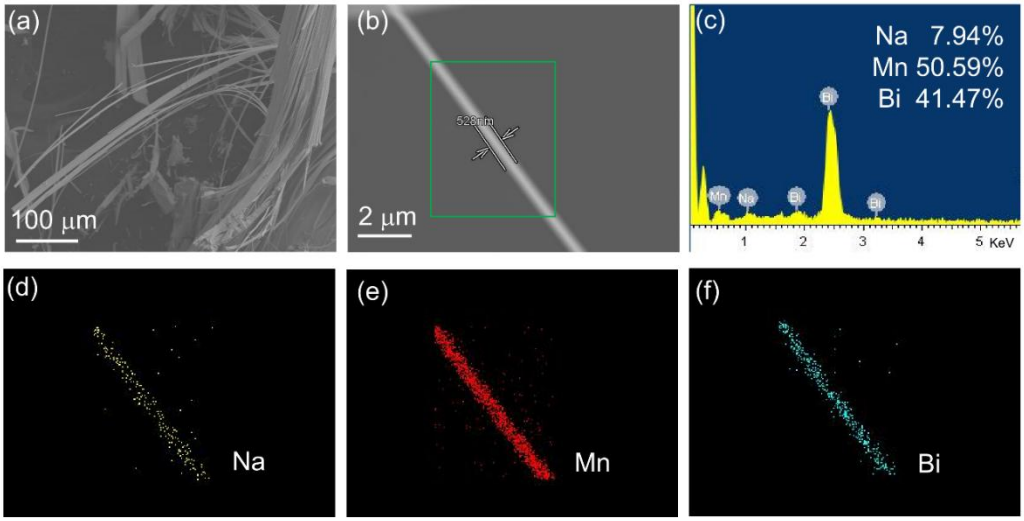


**Fig. S1** Quasi-one-dimensional feature of $NaMn_6Bi_5$. SEM image of $NaMn_6Bi_5$ at a scale of (a) 100 μm and (b) 2 μm. Elemental analysis (c) and elemental mapping for (d) Na, (e) Mn, and (f) Bi by energy-dispersive spectroscopy on the wire.

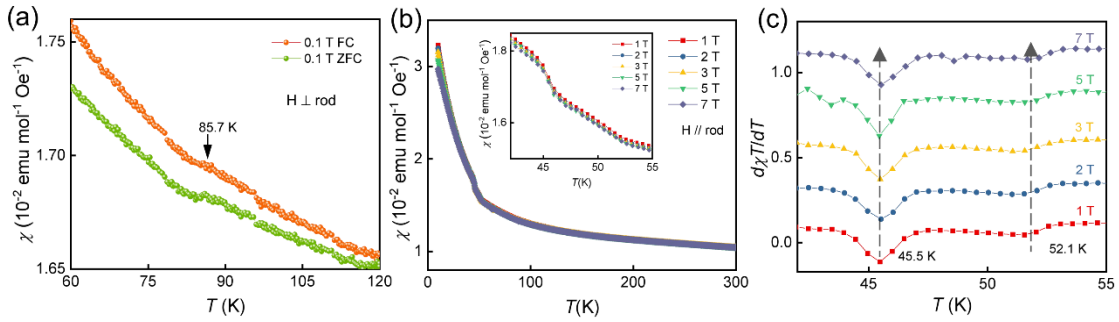


**Fig. S2** (a) Zoomed susceptibility from 60 K to 120 K for $H \perp$ rod. The black arrow donates the small kink at 85.7 K. (b) Temperature dependent magnetic susceptibility of $NaMn_6Bi_5$ single crystal under various magnetic field for $H$ // rod. The inset is the zoomed susceptibility around 50 K. (c) The $d\chi T/dT$ curves in the temperature range 42 K - 55 K, showing almost unchanged magnetic transition temperatures with increasing magnetic field.

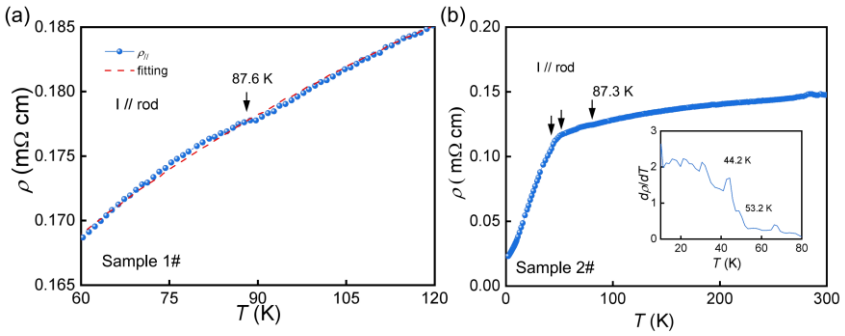


**Fig. S3** (a) Zoomed resistivity from 60 K to 120 K for $I$ // rod. The black arrow donates the small kink at 87.6 K. (b) Temperature dependent resistivity of another $NaMn_6Bi_5$ single crystal (Sample 2#). The inset is the first derivative in the temperature range 10 K - 80 K.

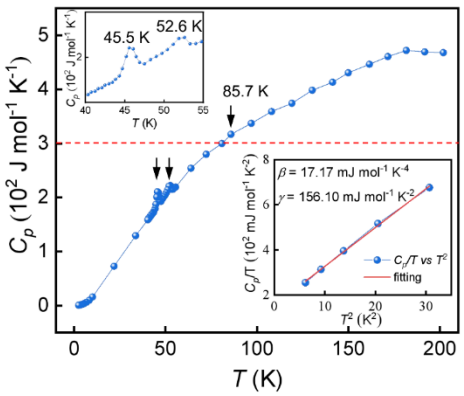


**Fig. S4** Temperature dependent specific heat capacity of another $NaMn_6Bi_5$ single crystal and the corresponding linear fitting at low temperature range by using Debye model.